Supplementary Materials

Tuning Ni–O/Ni–S coordination for efficient electrocatalytic oxidation of 5-hydroxymethylfurfural to 2,5-furandicarboxylic acid

Wen Guan [a], Chao Xu [a], Yao Chen [b], Yanli Mao [c], Zhongxian Song*[c], Binrong Li*[d], Yongsheng Yan [a] and Yunlei Zhang*[a]

[a] Institute of Green Chemistry and Chemical Technology, School of Chemistry and Chemical Engineering, Jiangsu University, Xuefu Road 301, Zhenjiang 212013, P. R. China

[b] School of the Environment and Safety, Jiangsu University, Xuefu Road 301, Zhenjiang 212013, P. R. China.

[c] Faculty of Environmental and Municipal Engineering, Henan University of Urban Construction, Pingdingshan 467000, P. R. China

[d] School of Environmental Science and Engineering, Suzhou University of Science and Technology, Suzhou 215009, P.R. China.

Experimental section

Materials

All of the chemicals used in the reaction were analytical grade and not further purified. Nickel(II) chloride hexahydrate ($NiCl_2·6H_2O$, AR, ＞98%), 2,5-thiophenedicarboxylic acid ($C_6H_4O_4S$, ≥99.8%), sodium hydroxide (NaOH, AR, ≥99.0%), potassium hydroxide (KOH, AR, ≥99.0%) were all purchased from Sinopharm Reagent Co., Ltd. (China). 5-Hydroxymethylfurfural (HMF, AR, >99.0%), 2,5-furandicarboxylic acid (FDCA, AR, >99.0%), 5-hydroxymethyl-2-furancarboxylic acid (HMFCA, AR, >99.0%), 5-formyl-2-furoic Acid (FFCA, AR, >99.0%), acetic acid (CH_3COOH, HPLC, ≥99.8%), acetonitrile (C_2H_3N, AR, >99.0%) were purchased from Aladdin Reagent Co., Ltd. (Shanghai, China). Nickel foam (NF, 1.0 mm thickness) was provided by Suzhou Kesheng and Metal Materials Co., Ltd. (China).

Synthesis of Ni-T catalysts

NF (1 × 2 cm^2) was ultrasonically cleaned sequentially with acetone, 3 M HCl, and deionized water, after which it was dried in a vacuum oven at 60 ℃ overnight. Subsequently, 20 mL of an aqueous solution containing 0.33 mmol $NiCl_2·6H_2O$, 1 mmol $C_6H_4O_4S$ and 2 mmol NaOH was added to 100 mL of a polytetrafluoroethylene-lined container. After stirring evenly, it was placed in a hydrothermal reactor, and washed with the cleaned NF. The reaction was carried out at 180℃ for 22 hours. After the reaction, the NF was rinsed with deionized water until the pH was 7. It was then placed in a 70℃ oven for drying to obtain $Ni(OH)_2$. The $Ni(OH)_2$ was heated in a tube furnace at a rate of 5℃/min to 200℃ and kept for 2 hours to obtain the Ni-200℃ catalyst. By changing the calcination temperature to 300℃, 400℃ and 500℃, the Ni-300℃, Ni-400℃ and Ni-500℃ catalysts were obtained.

Characterization

X-ray diffraction (XRD) patterns were recorded on a Bruker D8 diffractometer with Cu *K*α radiation, using a scanning range of 10°-80° at a speed of 5° min^{-1}. The images of samples were obtained by scanning electron microscopy (SEM JSM-7500F, JEOL, Japan), transmission electron microscopy (TEM, HT7800),

and high-resolution TEM (HRTEM) (FEI Tecnai G2F20). Nitrogen adsorption-desorption isotherms were measured on a BELSORP-mini X apparatus. The specific surface area was determined using the Brunauer–Emmett–Teller (BET) method, and pore size distributions were calculated from the desorption branch of the isotherm using the Barrett–Joyner–Halenda (BJH) model. X-ray photoelectron spectroscopy (XPS) measurements were conducted on a Thermo Fisher Scientific ESCALAB 250 instrument with a monochromated Al X-ray source. All XPS results were calibrated by setting the C 1s peak to 284.6 eV. X-ray absorption fine structure (XAFS) spectroscopy was performed in transmission mode using a Rapid-XAFS 1M spectrometer (Anhui Absorption Spectroscopy Analysis Instrument Co., Ltd.) operated at 25 kV and 40 mA. A Si (533) spherical bending crystal analyser with a radius of curvature of 500 mm was used for the analysis of the Ni sample.

Data reduction, data analysis, and fitting of EXAFS fitting were performed using the Athena and Artemis programs of the Demeter data analysis packages, which employs the FEFF6 code to model EXAFS spectra. Energy calibration was carried out using a standard Ni foil standard measured simultaneously as a reference. A linear pre-edge background was subtracted, and the absorption edge was normalized using Athena. The $\chi(k)$ function was extracted by subtracting a smooth, third-order polynomial atomic background. The k^3-weighted $\chi(k)$ data were Fourier transformed over a k-range of 1.0 $Å^{-1}$ using a Hanning window. EXAFS fitting was conducted in R-space via least-squares refinement in Artemis, with global parameters (coordination number CN, bond distance R, Debye–Waller factor σ^2, and energy shift ΔE_0) adjusted to fit the theoretical model to the experimental data. The amplitude reduction factor ($S_0^2 = 0.753$) was determined from fitting the Ni foil standard and subsequently fixed during the analysis of Ni–O, Ni–S, and Ni–O–S scattering paths in the sample.

Electrochemical test

All electrochemical measurements for HMF oxidation were carried out on a CHI-660E electrochemical workstation (CH Instruments Inc., Shanghai) in a three-electrode

mode at room temperature. The working electrode was the Ni-200℃, Ni-300℃, Ni-400℃, and Ni-500℃ (1 × 2 cm^2). Pt sheet (1 × 1 cm^2) and Ag/AgCl (3 M KCl) were used as the counter and reference electrodes, respectively. The measured potentials were referenced to the reversible hydrogen electrode (RHE) according to the following equation:

$$E_{RHE} = E_{Ag/AgCl} + 0.0591 \times pH + 0.197 \quad (1)$$

The electrochemical HMF oxidation was conducted in 40 mL electrolyte consisting of 0.1 M KOH.

Product analysis

The products from the electrochemical HMF oxidation were determined and analyzed by HPLC (Agilent 1260 Infinity II, Agilent Technologies) equipped with an Agilent C18 column. 0.1 wt% CH_3COOH solution and C_2H_3N (v:v=92:8) was used as the eluent with a constant flow rate of 0.6 mL·min^{-1}, and the temperature of the column was maintained at 30 °C. The products, including HMFCA, FFCA, and FDCA were analyzed following chronoamperometry at various potentials for 4 hours.

$$HMF\ Conversion = \frac{mole\ of\ HMF\ consumed}{mole\ of\ initial\ HMF} \times 100 \quad (2)$$

$$HMFCA\ or\ FFCA\ or\ FDCA\ Selectivity = \frac{mole\ of\ HMFCA\ or\ FFCA\ or\ FDCA\ formed}{mole\ of\ initial\ HMF} \times 100\% \quad (3)$$

$$FDCA\ FE = \frac{mol\ of\ FDCA\ formed}{total\ charge/(6 \times F)} \times 100\% \quad (4)$$

F represents the faraday constant, with a value of 96485 C/mol.

Computational detail

Discrete Fourier Transform (DFT) calculation were conducted through the Vienna ab initio Simulation Package (VASP) with the projector augment wave method[1,2]. Generalized gradient approximation of the Perdew-Burke-Ernzerhof (PBE) functional was used as the exchange-correlation functional[3]. The Brillouin zone was sampled with 2 × 2 × 1 K points for surface calculation[4]. The cutoff energy was set as 500 eV, and structure relaxation was performed until the convergence criteria of energy and force reached 1 × 10^{-5} eV and 0.02 eV $Å^{-1}$, respectively. A vacuum layer of 15 Å was

constructed to eliminate interactions between periodic structures of surface models. The van der Waals (vdW) interaction was amended by the zero damping DFT-D3 method of Grimme[5].

The adsorption energy (ΔE_{ads}) of adsorbate adsorption on surface is defined as

$\Delta E_{ads} = E(*adsorbate) - E(*) - E(adsorbate)$

where E(*adsorbate) and E(*) are the total energy of surface systems with and without adsorbate, respectively, E(adsorbate) is the energy of an isolated adsorbate. According to this definition, negative adsorption energy suggests that the adsorption process is exothermic and the adsorption system is thermodynamically stable. Contrarily, a positive value corresponds to an endothermic and unstable adsorption.

The Gibbs free energy was calculated as $\Delta G = \Delta E + \Delta E_{ZPE} - T\Delta S$, where the ΔE, ΔE_{ZPE}, and ΔS are electronic energy, zero-point energy, and entropy difference between products and reactants. The zero-point energies of isolated and absorbed intermediate products were calculated from the frequency analysis[5]. The vibrational frequencies and entropies of molecules in the gas phase were obtained from the National Institute of Standards and Technology (NIST) database[6,7].

In-situ attenuated total reflection infrared (ATR-FTIR) measurements

The ATR-FTIR spectrometer was based on the Nicolet iS10 spectrometer with a high-sensitivity MCT detector and a heating chamber with a ZnSe window. Firstly, the catalyst was dissolved in ethanol, and then the suspension was coated on the crystal surface of the glass carbon electrode, the electrochemical reaction tank accessories were assembled, and 3 mL of KOH electrolyte was added. Stand for 15 min until the system becomes stable. At this time, ATR-FTIR spectra were recorded with an average of 32 scans, and the resolution was 4 cm^{-1}. After the background of the solution was deducted, the FF solution was injected at the same time, the catalyst was adsorbed for 30 min, and the original ATR-FTIR spectra of the solid-liquid surface were recorded.

In-situ NAP-XPS experiments

The near-ambient pressure X-ray photoelectron spectroscopy (NAPXPS) experiments were conducted on a laboratory-based SPECS nearambient pressure XPS system (base pressure <5 × 10−10mbar) with a monochromatic Al Kα X-ray source,

equipped with a glovebox linked to a vacuum system. The Ni-300°C catalyst performed electrochemical reactions in a KOH electrolyte at 1.66 V vs. RHE and pH 13. XPS analyses were performed at specific time intervals during the reaction. All NAP-XPS spectra were calibrated to the C 1s peak at 284.6 eV.

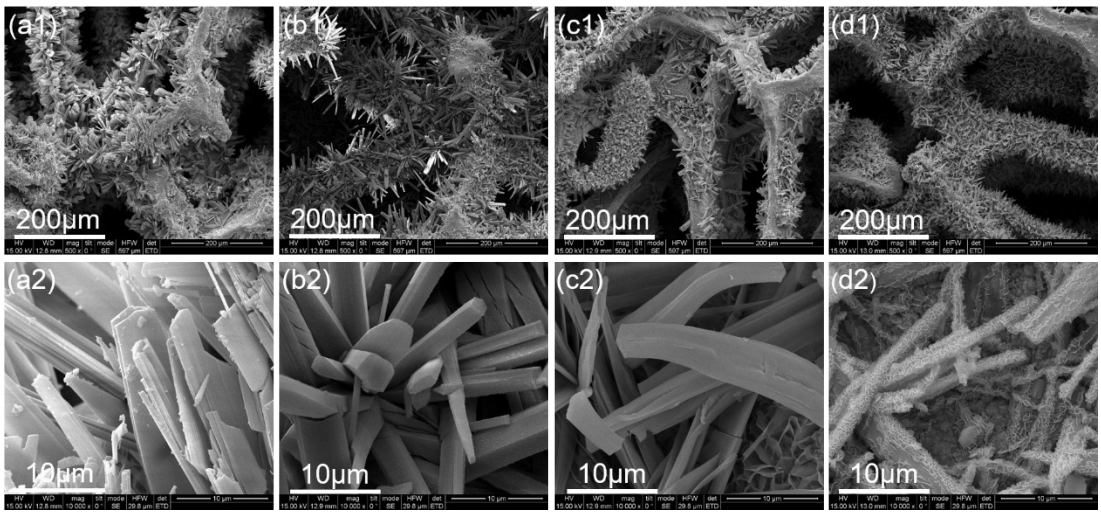

Fig. S1. SEM images of (a) Ni-200℃, (b) Ni-300℃, (c) Ni-400℃, and (d) Ni-500℃.

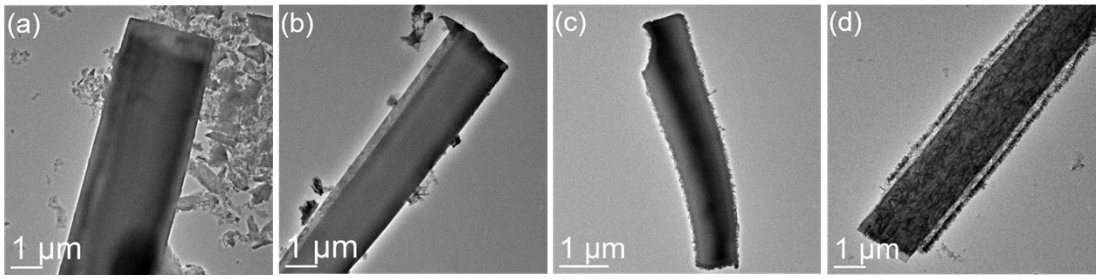

Fig. S2. TEM images of (a) Ni-200℃, (b) Ni-300℃, (c) Ni-400℃, and (d) Ni-500℃.

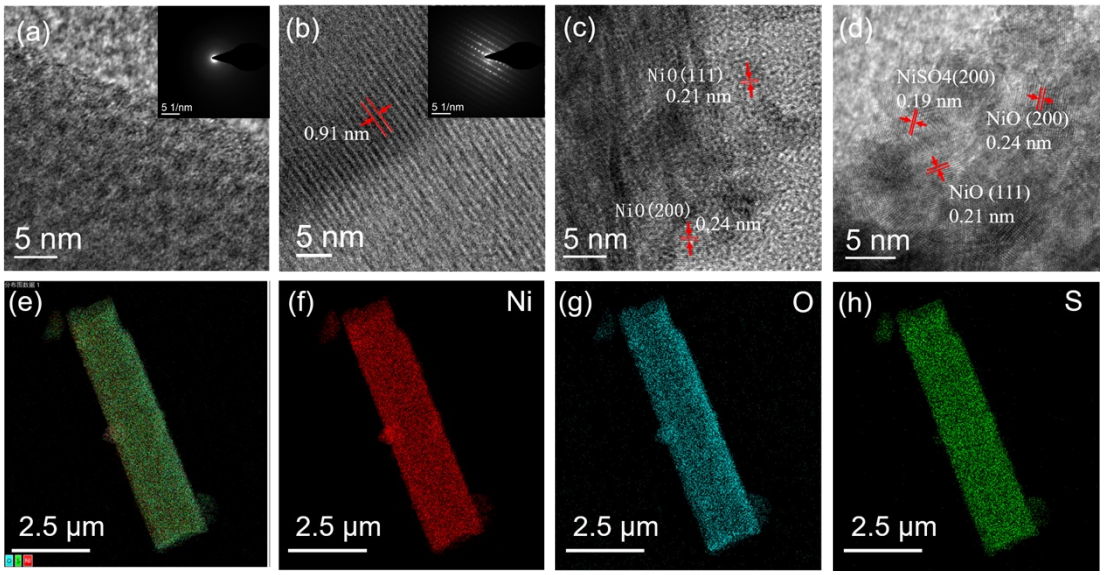

Fig. S3. HRTEM images of (a) Ni-200℃, (b) Ni-300℃, (c) Ni-400℃, (d) and Ni-500℃. (e) EDS elemental mapping images of the (f) Ni, (g) O, and (h) S elements for Ni-300℃.

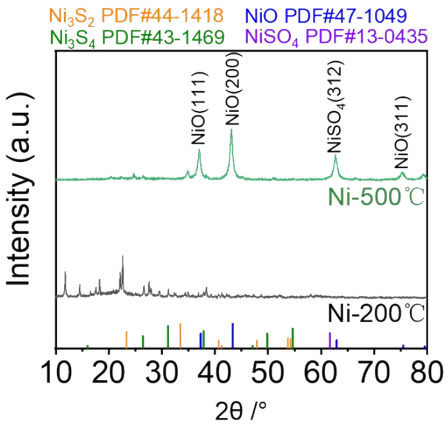

Fig. S4. The XRD of Ni-200 ℃ and Ni-500 ℃.

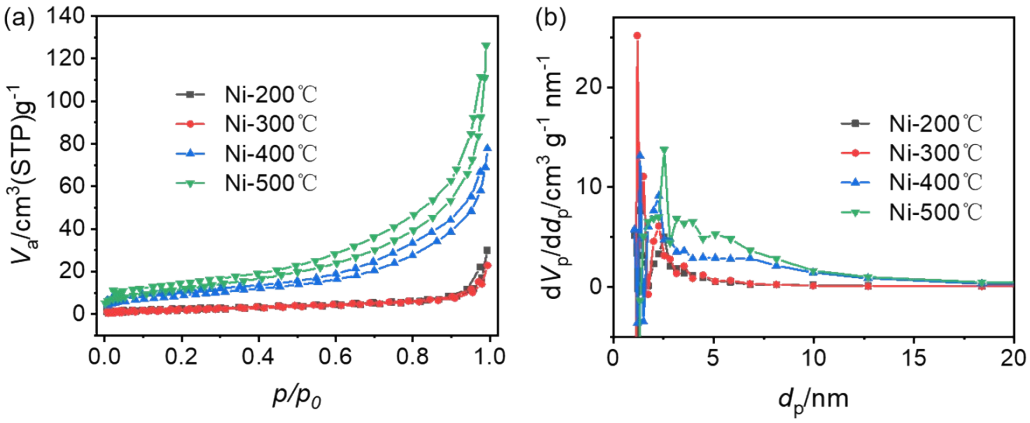

Fig. S5. The (a) Nitrogen adsorption–desorption isotherms and (b) diameter distribution graph of Ni-200 ℃, Ni-300 ℃, Ni-400 ℃, and Ni-500 ℃.

Table S1. Pore structure of Ni-200 ℃, Ni-300 ℃, Ni-400 ℃, and Ni-500 ℃.

Sample	S_{BET}[a] (m^2 g^{-1})	D_{BJH}[b] (nm)	V_t[c] (cm^3 g^{-1})
Ni-200 ℃	7.28	13.854	0.043462
Ni-300 ℃	8.1322	14.6	0.036604
Ni-400 ℃	32.819	11.545	0.1172
Ni-500 ℃	44.286	16.304	0.1895

S_{BET}[a] is the BET specific surface area. D_{BJH}[b] is the BJH mean pore diameter calculated by the desorption branches of the nitrogen sorption isotherms. V_t[c] is the total pore volume determined at a relative pressure of 0.99.

Table S2. The sulfur content of the Ni-200°C, Ni-300°C, Ni-400°C, and Ni-500°C.

	Ni-200°C	Ni-300°C	Ni-400°C	Ni-500°C
S content (wt%)	9.0509	7.0948	4.4614	0

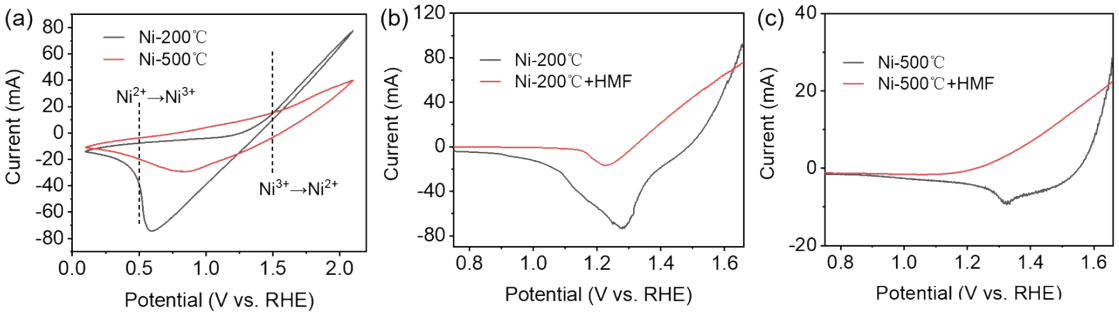

Fig. S6. (a) Cyclic voltammograms (CVs) of Ni-200°C and Ni-500°C using 0.1 M KOH as supporting electrolyte with and without HMF solution. Linear sweep voltammograms (LSVs) of (b) Ni-200°C and (c) Ni-500°C using 0.1 M KOH as supporting electrolyte with and without HMF solution.

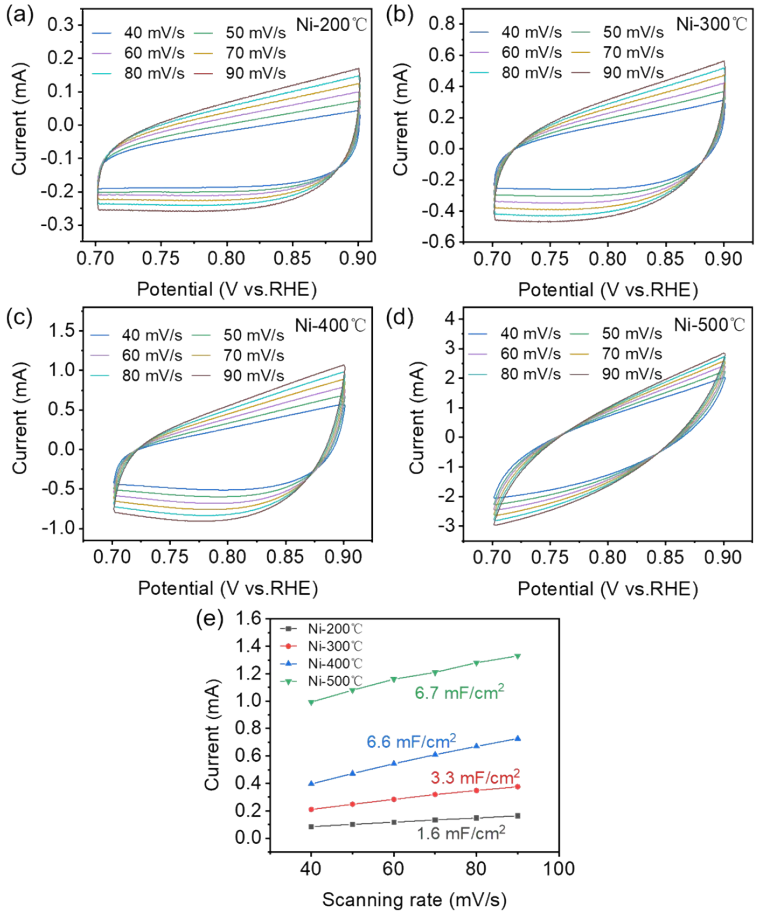

Fig. S7. CV curves of (a) Ni-200°C, (b) Ni-300°C, (c) Ni-400°C and (d) Ni-500°C at

different scan rates. (e) Charging current density vs. scan rates of 200℃, Ni-300℃, Ni-400℃ and Ni-500℃.

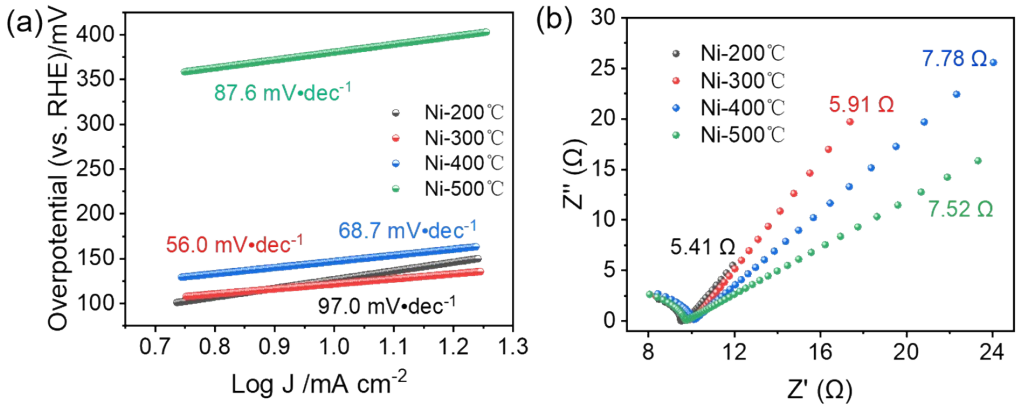

Fig. S8. (a) The Tafel slopes of Ni-200℃, Ni-300℃, Ni-400℃, and Ni-500℃. (b) The EIS plot of Ni-200℃, Ni-300℃, Ni-400℃, and Ni-500℃.

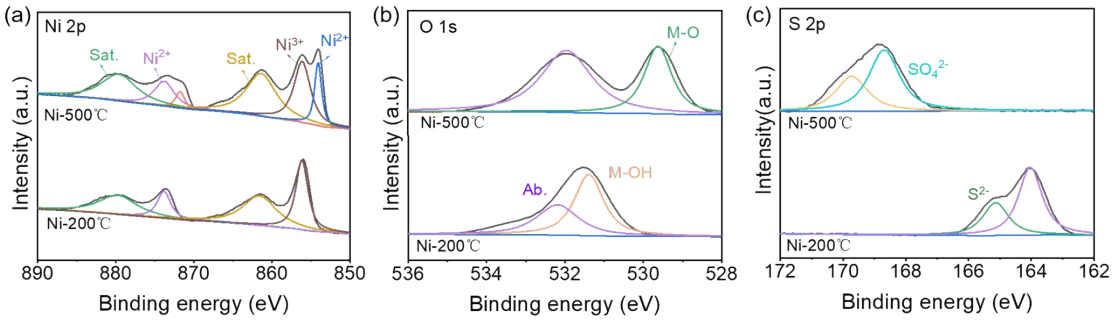

Fig. S9. The (a) Ni 2p, (b) O 1s, and (c) S 2p XPS spectras of Ni-200℃ and Ni-500℃.

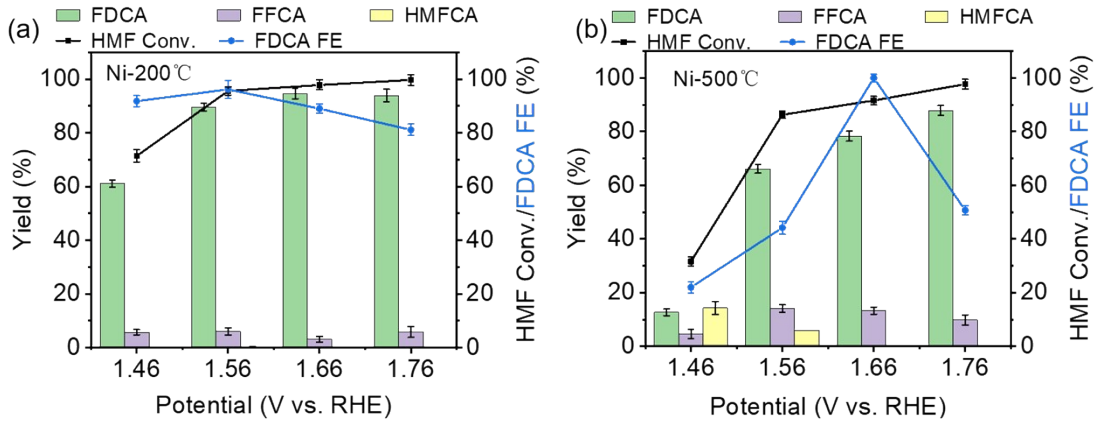

Fig. S10. The catalytic conversion of (a) Ni-200℃ and (a) Ni-500℃ catalysts at different potential (recorded in a 0.1 M KOH solution, 10 mM HMF).

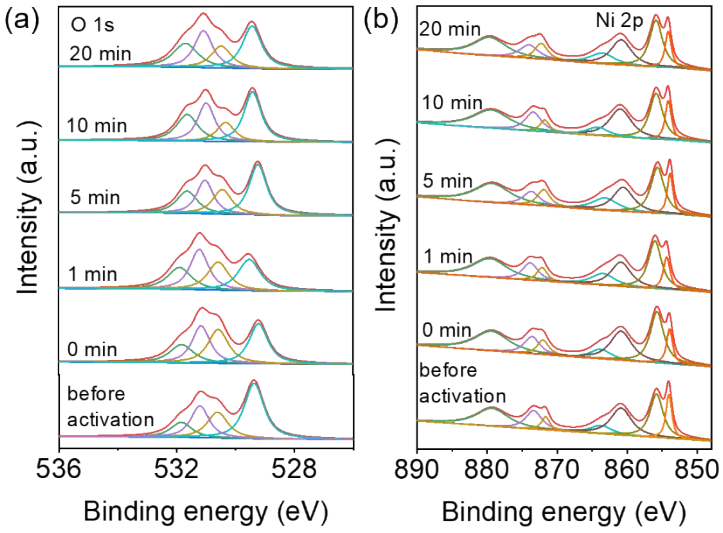

Fig. S11. In-situ XPS spectra of (a) O 1s, and (b) Ni 2p at the oxidation potential of Ni-300℃ (1.66 V vs. RHE).

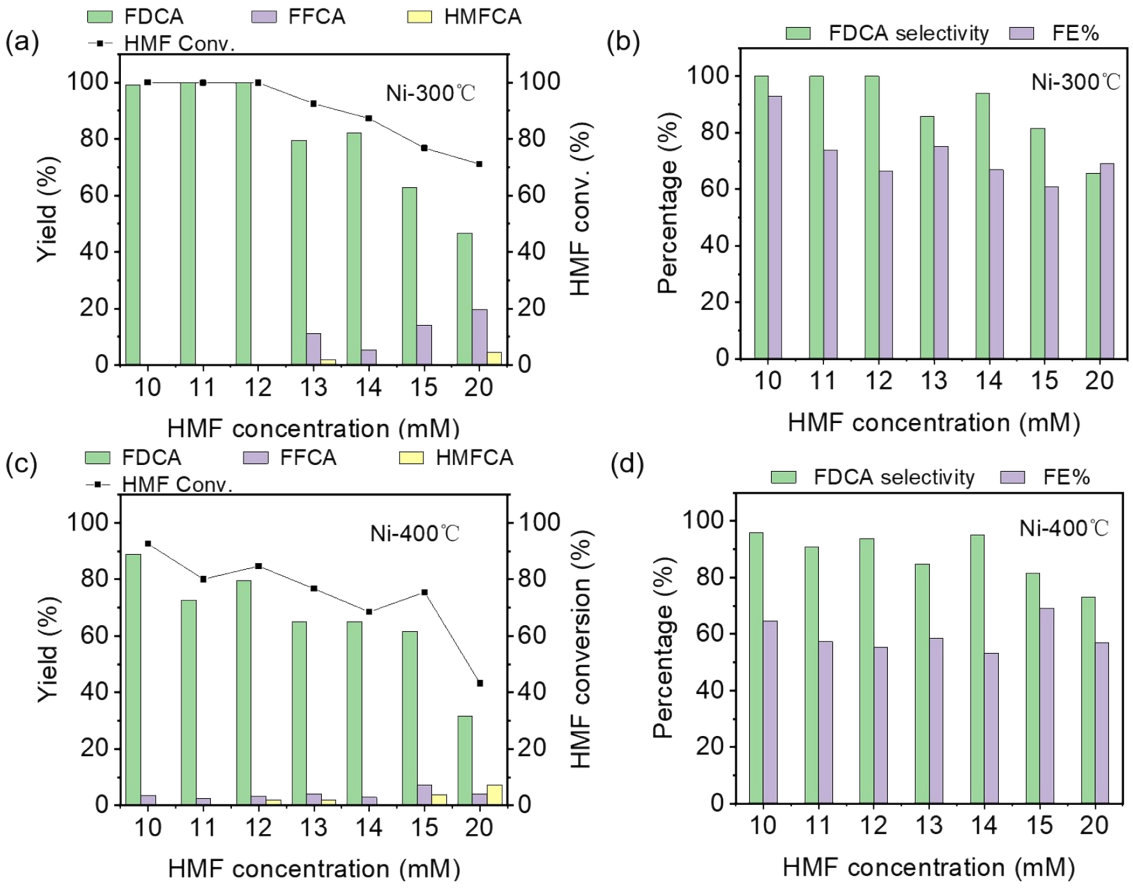

Fig. S12. (a-b) The catalytic performance of Ni-300℃ in different HMF concentrations and the selectivity of FDCA and FE. (c-d) The catalytic performance of Ni-400℃ in different HMF concentrations and the selectivity of FDCA and FE.

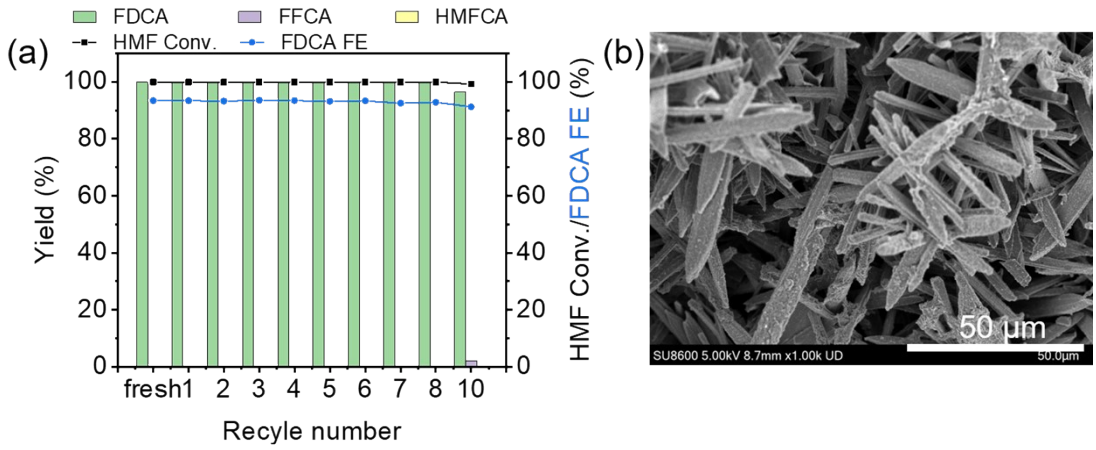

Figure S13. (a) The catalytic performance and (b) SEM image of the Ni-300℃ catalyst after 10 cycles of reuse (1.66 V vs. RHE, 4 h).

Table S3. The content of Ni and S in the electrolyte during the cyclic test process.

elements content	1	2	3	4	5	6	7	8	9	10
Ni (mg/L)	0.12	0.09	0.11	0.11	0.11	0.11	0.10	0.11	0.10	0.12
S (mg/L)	0	0	0	0	0	0	0	0	0	0

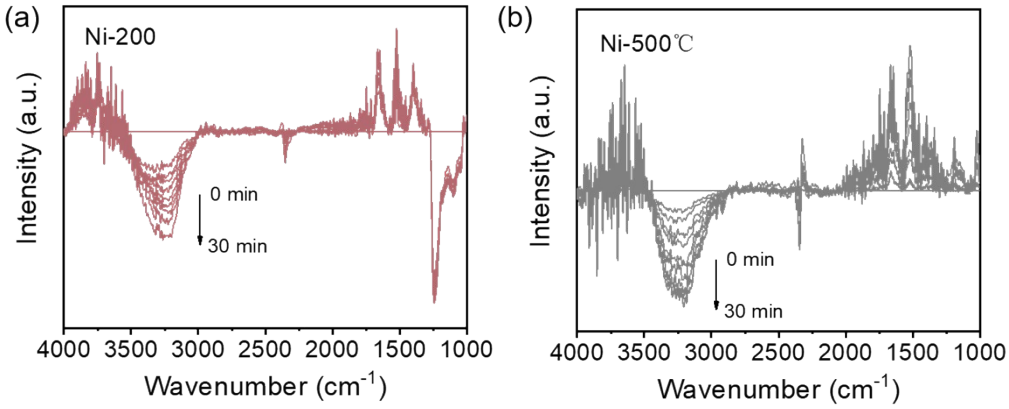

Fig. S14. In situ infrared spectra of HMF adsorbed on the catalyst surfaces at (a) Ni-200℃, and (b) Ni-500℃.

Table S4. EXAFS fitting parameters at the Ni K-edge for Ni-300℃ and Ni-400℃ (S_0^2=0.85 from Ni-foil).

	shell	CN[a]	R[b](Å)	σ^{2c}(Å^2)	ΔE_0[d](eV)	R factor
Ni-300℃	Ni-O	4.08±0.1	2.09±0.01	0.0136	-3.5±0.1	0.007
	Ni-S	1.44±0.1	2.36±0.01	0.0140		
	Ni-O-Ni	2.53±0.1	3.00±0.02	0.0084		
	Ni-S-Ni	1.73±0.1	3.85±0.09	0.0095		
Ni-400℃	Ni-O	5.73±0.4	2.07±0.02	0.0097	-3.6±0.3	0.015
	Ni-S	1.38±0.1	2.29±0.06	0.0150		
	Ni-O-Ni	10.02±0.5	2.96±0.02	0.0096		
	Ni-S-Ni	1.26±0.2	3.92±0.04	0.0074		

Table S5. The free energy of NiO and NiO-S surfaces in different states

	G_0 (eV)	NiO		NiO-S	
		E (eV)	G (eV)	E (eV)	G (eV)
Slab	-	-545.84	0	-515.26	0
HMF	-90.49	-638.12	-1.78	-608.98	-3.22
HMFCA	-97.90	-638.83	-2.09	-616.42	-3.26
FFCA	-94.77	-642.41	-1.80	-612.82	-2.78
FDCA	-102.27	-649.56	-1.44	-620.13	-2.59

References

[1] G. Kresse, D. Joubert, *Phys. Rev. B*, 1999, **59**, 1758-1775.

[2] P.E. Blöchl, *Phys. Rev. B*, 1994, **50**, 17953-17979.

[3] J.P. Perdew, K. Burke, M. Ernzerhof, *Phys. Rev. Lett.*, 1996, **77**, 3865-3868.

[4] V. WANG, N. XU, J.-C. LIU, et al., *Comput. Phys. Commun.*, 2021, **267**, 108033.

[5] S. Grimme, S. Ehrlich, L. Goerigk, *J. Comput. Chem.*, 2011, **32**, 1456-1465.

[6] J.K. Nørskov, J. Rossmeisl, A. Logadottir, et al., *J. Phys. Chem. B*, 2004, **108**, 17886-17892.

[7] J.K. Nørskov, T. Bligaard, A. Logadottir, et al., *J. Electrochem*. Soc. 2005, **152**.